

Electronic Supplementary Material (ESI) for Materials Horizons.
This journal is © The Royal Society of Chemistry 2018

Intramolecular Electronic Coupling for Persistent Room-Temperature Luminescence

for Smartphone Based Time-Gated Fingerprints Detection

*Di Tian,^a Zece Zhu,^{*a} Li Xu,^{*b} Hengjiang Cong,^c Jintao Zhu^{*a}*

^aKey Lab of Materials Chemistry for Energy Conversion and Storage of Ministry of Education, School of Chemistry and Chemical Engineering, Wuhan National Laboratory for Optoelectronics, Huazhong University of Science and Technology, Wuhan 430074, P. R. China. E-mail: jtzhu@mail.hust.edu.cn (J. Zhu); zece@hust.edu.cn (Z. Zhu)

^bDepartment of Pharmacy, Hubei University of Chinese Medicine, Wuhan 430065, P. R. China. E-mail: xuli81819009@126.com

^cDepartment of Chemistry, Wuhan University, Wuhan 430072, P. R. China.

Experimental Section

General information: p-CzDPS^{S1,2} was purchased from Xi'an Polymer Light Technology Corp. ¹H NMR and ¹³C NMR spectra were recorded using MERCURYVX300 and Bruker Advanced II (400 MHz) spectrometers. Mass spectra were collected by a Bruker micrOTOF-MS. UV-*vis* absorption spectra were recorded on a Shimadzu UV-2700 spectrophotometer. Phosphorescence spectra with a delay time over milliseconds were measured on a Hitachi F-4600 spectrophotometer. For measuring phosphorescence spectra and phosphorescence decays at 77K, samples were cooling in a Dewar flask filling with liquid N₂, and then were measured on a Hitachi F-4600 spectrophotometer. Other time-gated luminescence spectra were measured on Perkin Elmer LS 55 luminescence spectrometer. Phosphorescence decays over 10 s were measured on a Hitachi F-4600 spectrophotometer. Other luminescence decay was obtained from a single photon counting spectrometer on Edinburgh Instruments (FLS920) with a Picosecond Pulsed UV-LASTER (LASTER377) or a microsecond pulsed Xenon lamp (μF900) as the excitation light source.

The powder X-ray diffraction patterns were recorded by Rigaku MiniFlex 600 with an X-ray source of Cu K α ($\lambda = 1.5418 \text{ \AA}$) at 25 °C at 40 KV and 15 mA at a scan rate of 10° (2 θ)/min (scan range: 5-50°). The single-crystal X-ray diffraction data were obtained from a Bruker Smart Apex CCD diffractometer by using Mo/Cu K α radiation ($\lambda = 0.71073 \text{ \AA}$) with a $w/2\theta$ scan mode at 296 K. Structures of the crystals were analyzed by direct methods using the SHELXL-97 software. None-hydrogen atoms were refined anisotropically by full-matrix least-squares calculations on F2 using SHELXL-97, while the hydrogen atoms were directly introduced at calculated position and refined in the riding mode. Drawings were produced using ORTEP-3.

Synthesis of 9-9'-(sulfonylbis(2, 1-phenylene)) bis(9H-carbazole) (CzDPS): The key intermediates, bis(2-fluorophenyl)sulfone (*o*-DFSO₂) was synthesized according to our previous work.^{S3} The other chemicals were commercially available and used without further purification. A mixture of potassium carbonate (4.1 g, 30 mmol), carbazole (1.67 g, 10 mmol), and *o*-DFSO₂ (0.76 g, 3 mmol) in dry DMSO (10

mL) was heated to 150 °C and stirred for 24 h under argon. After the mixture was cooled to room temperature, the reaction was treated with brine and then extracted with dichloromethane for three times. The organic layers were collected and combined. Then, the solvent was removed by using rotary evaporators. The resulting product was purified by column chromatography on silica gel using n-hexane/dichloromethane as eluent to afford a pale-yellow powder (1.32 g, 80% yield). ¹H NMR (400 MHz, CDCl₃, δ ppm): 8.13 (d, J = 8 Hz, 4H), 7.44 (t, J = 8.6 Hz, 2H), 7.26 (t, J = 8 Hz, 4H), 7.17 (q, J = 8 Hz, 6H), 6.93 (d, J = 8 Hz, 2H), 6.73 (t, J = 8 Hz, 2H), 6.63 (d, J = 8 Hz, 4H); ¹³C NMR (125 MHz, CDCl₃, δ ppm): 142.82, 139.80, 136.56, 135.14, 132.14, 131.89, 129.30, 125.96, 123.44, 120.14, 110.38; EIMS *m/z* (%): [M]⁺ calcd. for C₃₆H₂₄N₂O₂S⁺ 548.16; found, 548.13; HRMS (ESI) *m/z*: [M+Na]⁺ calcd for C₃₆H₂₄N₂O₂SNa⁺, 571.1456; found 571.1473.

Computational study: Density functional theory (DFT) calculations were performed on Gaussian 09 program (Revision D09).^{S4} The ground state (S₀) geometries were optimized with the Becke's three-parameter exchange functional along with the Lee Yang Parr's correlation functional (B3LYP) using 6-31G(d) basis sets. The excitation energies in the n-th singlet (S_n) and n-th triplet (T_n) states were obtained using the TD-DFT method.

Preparing solidified tripropylene glycol diacrylate containing CzDPS: 1 mg CzDPS was dissolved in ~ 0.1 mL THF, then mixed with 0.1 g TRPGDA (Tripropylene glycol diacrylate) containing 1 wt% 2-hydroxy-4'-(2-hydroxyethoxy)-2-methylpropiophenone. The mixture was put in an 80 °C oven for 24 h for removing THF, and then was solidified under UV irradiation (365 nm LED, 200 mW).

Smartphone based time-gated finger imaging: The fresh fingerprints of volunteers on substrates were sprinkled with the powder crystals of CzDPS, and then shook the substrates gently to let the CzDPS powder adhere to the fingerprints. After blowing away the surplus powder crystals by an auralave, a Mi 4 phone equipped with a macro lens was used for imaging the substrates (Scheme S2). The steady-state images were

photographed under continuous illumination by a UV-LED (365 nm). The image with delayed luminescence was photographed immediately after turning off the UV-LED.

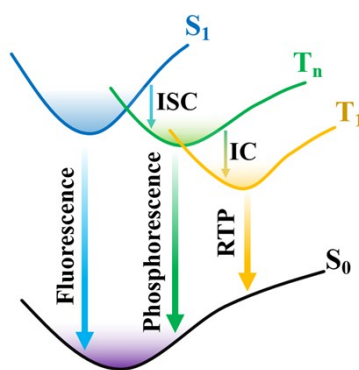
Supporting Movies:

Movie S1: The luminescence decay of different crystals of CzDPS.

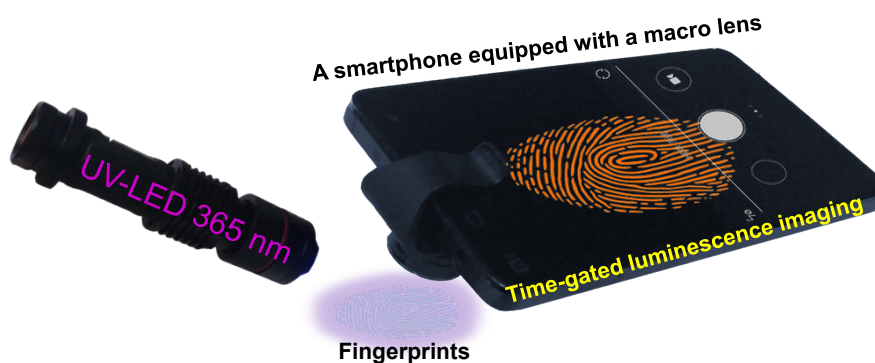
Movie S2: The luminescence decay of the *monoclinic* crystal of CzDPS in vacuum.

Movie S3: The luminescence of the solidified TRPGDA with 1 wt% CzDPS.

Supporting Figures:



Scheme S1. Schematic illustration showing the Jablonski diagram.^{S5,6} The ultra-long-lived excited state was attributed to the internal conversion (IC) from higher-order triplet states (T_n), which were transited from the excited singlet state through intersystem crossing.



Scheme S2. Time-gated luminescence imaging of fingerprints by using a smartphone.

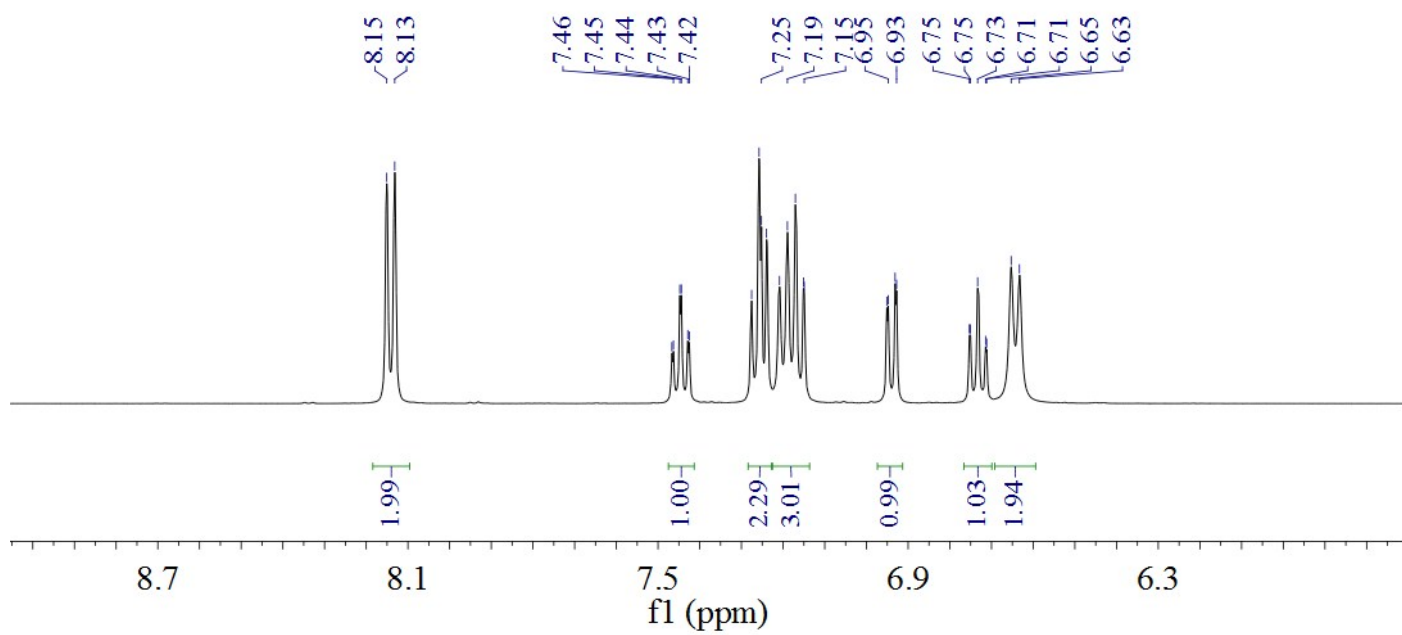


Figure S1. The ¹H-NMR spectrum of CzDPS.

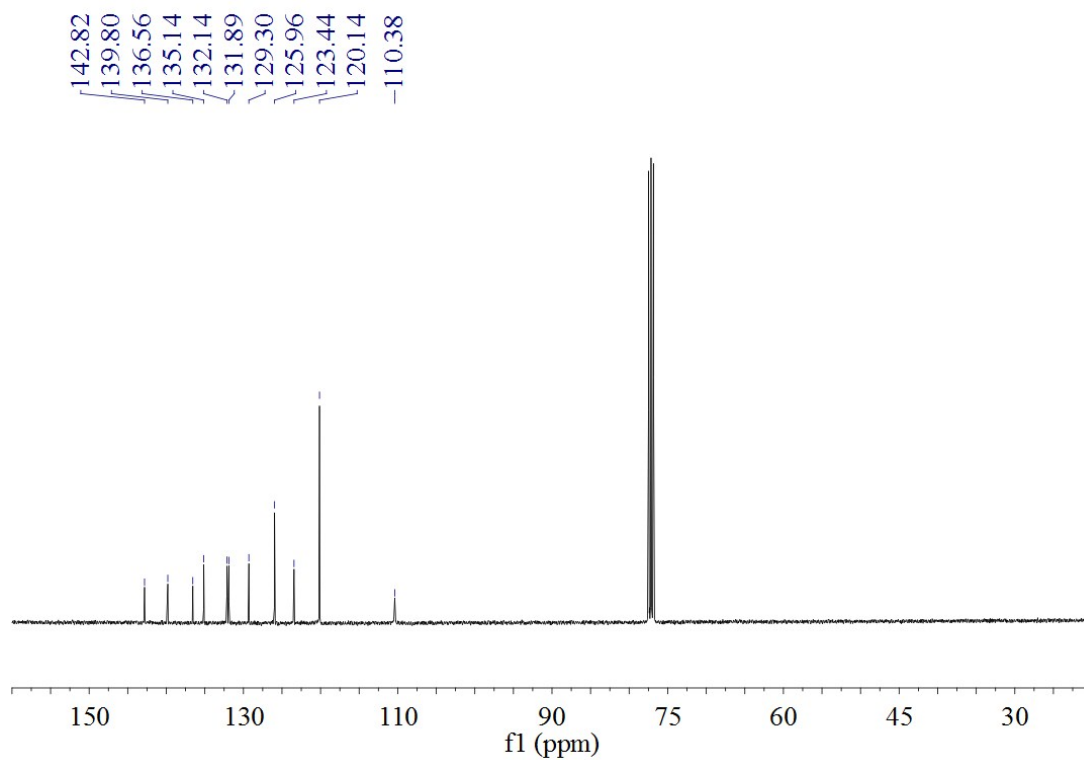


Figure S2. The ¹³C-NMR spectrum of CzDPS.

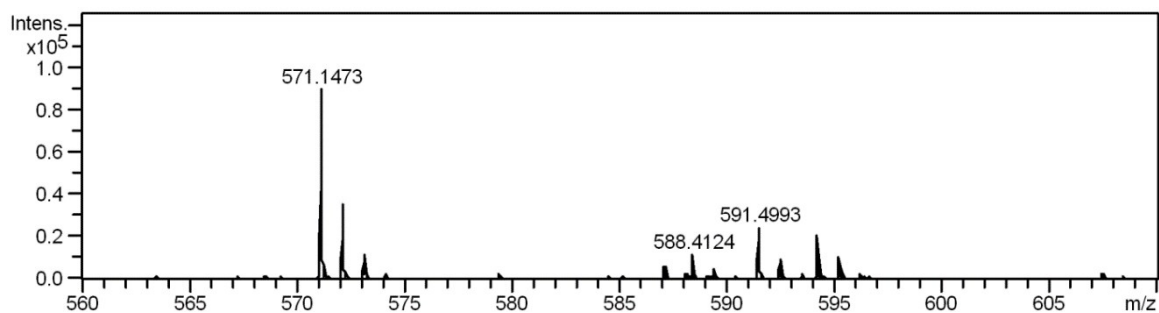


Figure S3. High resolution ESI mass spectrum of CzDPS. Calcd for $C_{36}H_{24}N_2O_2SNa^+$ $[M+Na]^+$ 571.1456, found 571.1473.

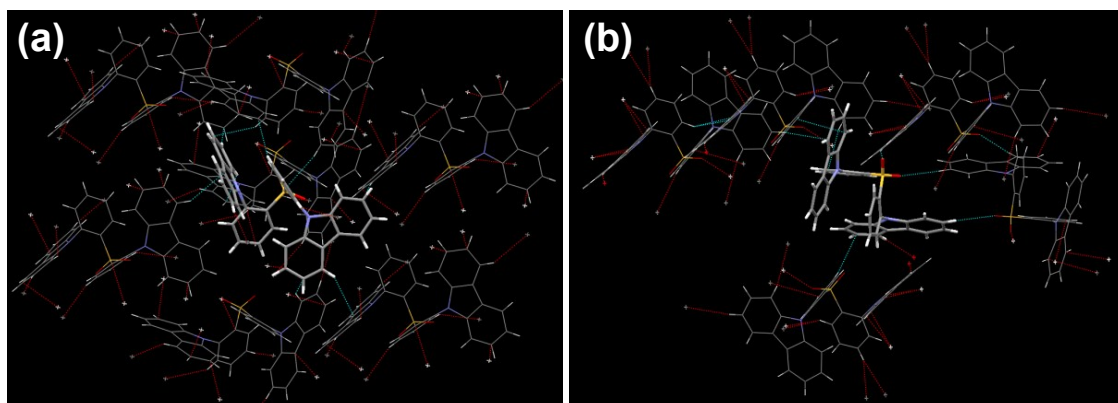


Figure S4. Intermolecular aggregation of CzDPS in the *orthorhombic* (a) and *monoclinic* (b) system. There was no strict intermolecular π - π stacking in either system.

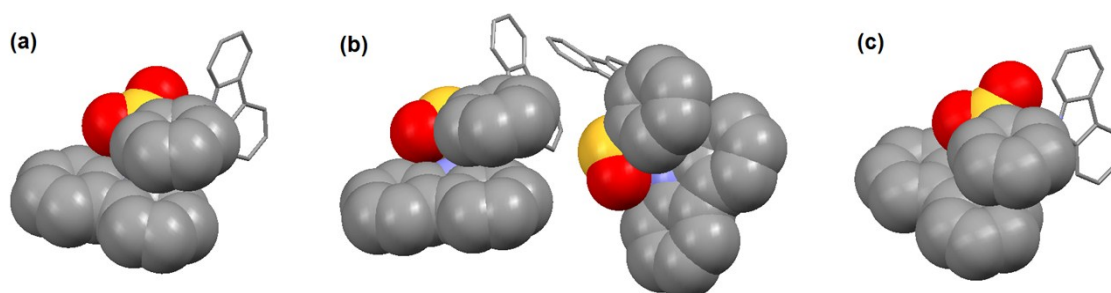


Figure S5. The molecular conformations of CzDPS in the orthorhombic (a), monoclinic (b) crystals and an optimized geometry (c) show the intramolecular interactions between phenylsulfone groups and carbazoyl rings. All the hydrogens were omitted.

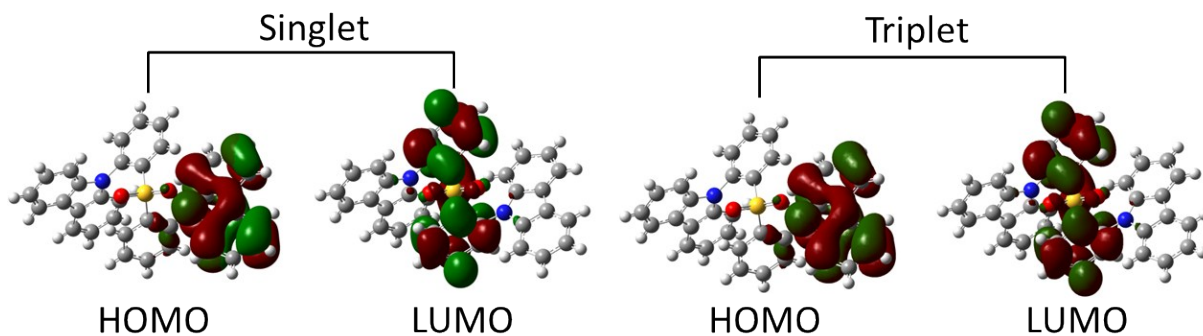


Figure S6. The HOMO, LUMO orbitals for the Czdps molecules. The ground state optimization was investigated by density functional theory at the B3LYP/6-31G(d) level.

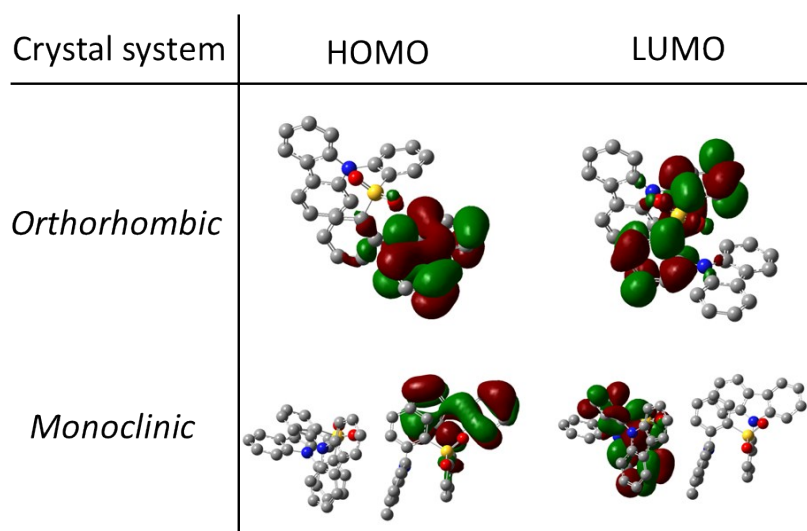


Figure S7. The calculated HOMO and LUMO of Czdps extracted from the *orthorhombic* and *monoclinic* system at the B3LYP/6-31G(d) level.

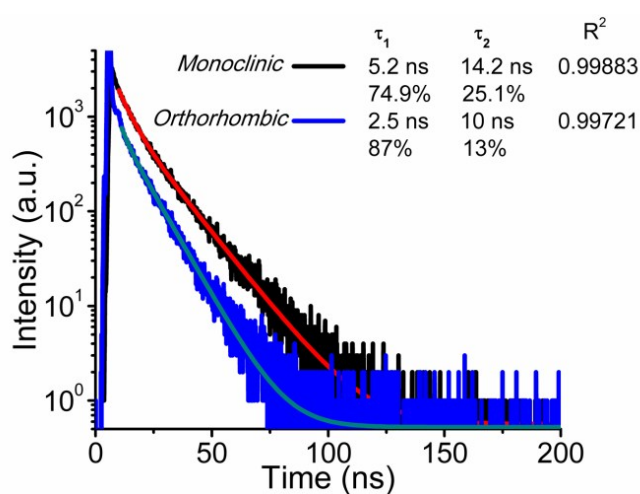


Figure S8. Luminescence decay of the *orthorhombic* and *monoclinic* crystals of Czdps at 420 nm at room temperature. The fluorescence lifetimes of both systems were only tens of nanoseconds.

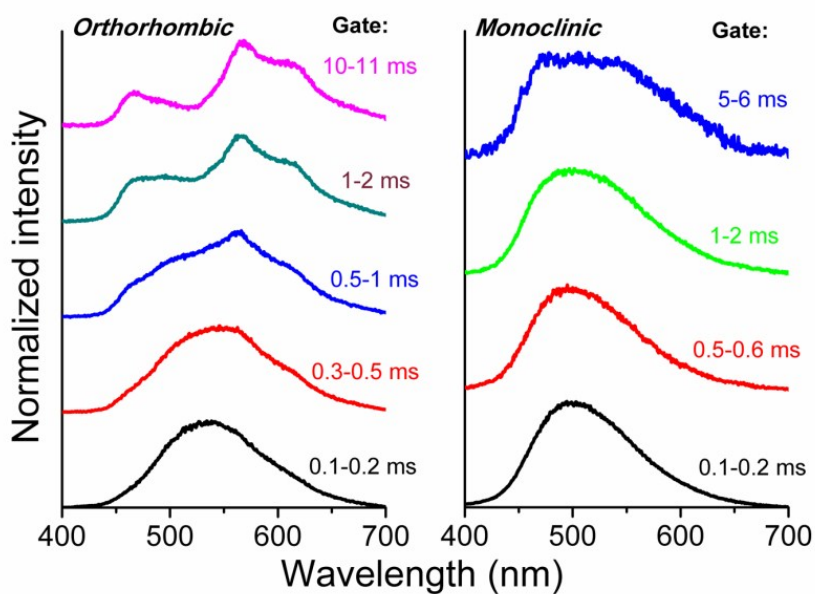


Figure S9. Time-gated luminescence spectra of the *orthorhombic* (a) and *monoclinic* (b) crystals ($\lambda_{\text{ex}} = 370$ nm). The phosphorescence emission peak at 500 ~ 530 nm suggested a shorter excited state in both crystals at room temperature.

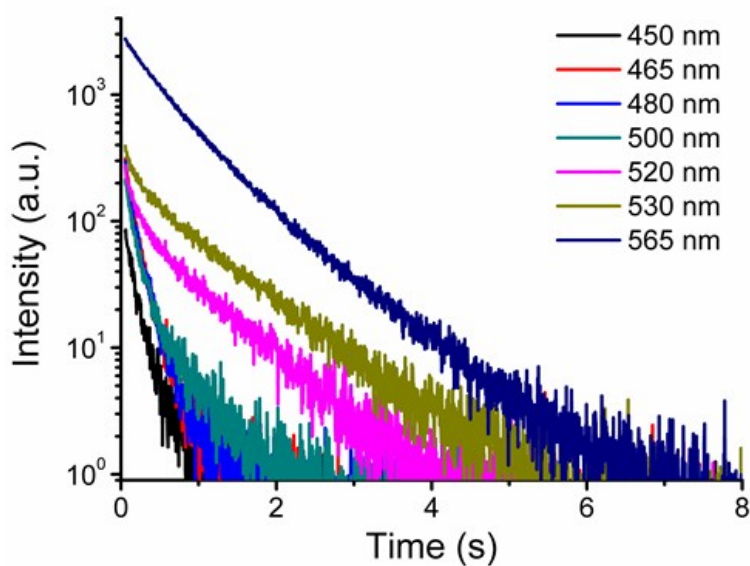


Figure S10. Luminescence decay of the *orthorhombic* crystal of CzDPS at room temperature. The emission at 500 ~ 530 nm showed longer lifetimes than that at 465 ~ 500 nm.

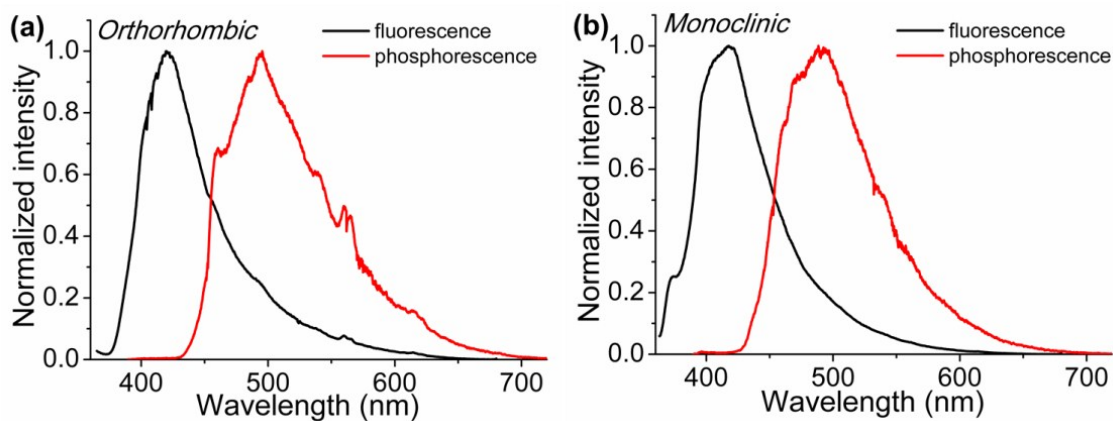


Figure S11. Fluorescence and phosphorescence spectra of the *orthorhombic* (a) and *monoclinic* (b) crystals at 77K. The phosphorescence emission of both crystals at ~ 500 nm became the major component at 77K.

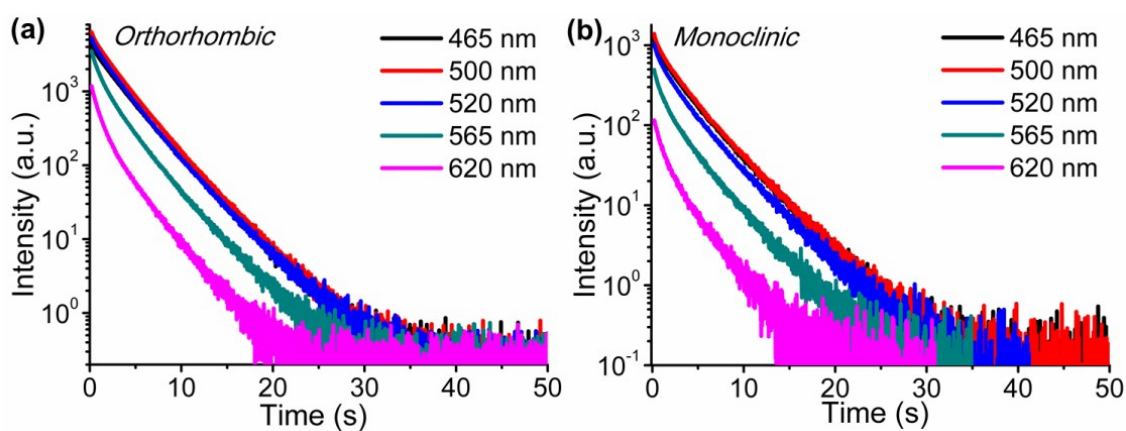


Figure S12. Luminescence decay of the *orthorhombic* (a) and *monoclinic* (b) crystal of CzDPS at 77K. Luminescence decay at ~ 500 nm was slower than that at other wavelength.

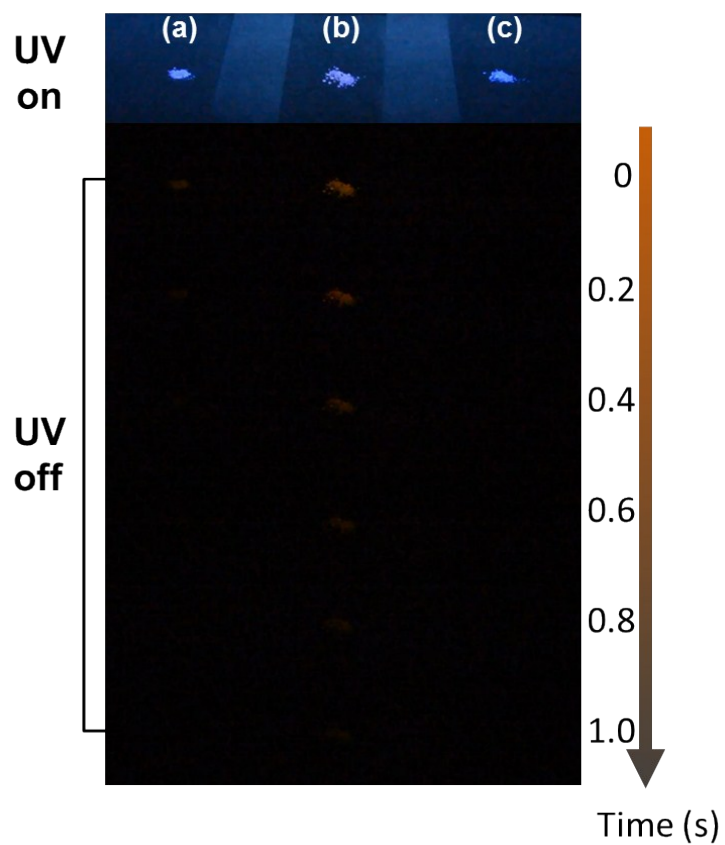


Figure S13. The images of powder crystal (a), *orthorhombic* (b) and *monoclinic* (c) systems of CzDPS under a UV light, and after turning off the UV light. Only powder and *orthorhombic* crystals showed persistent room-temperature luminescence.

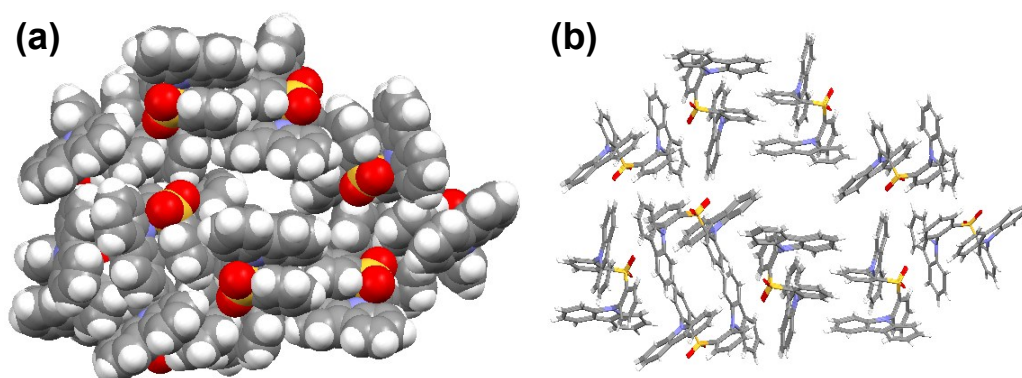


Figure S14. The micropore in *monoclinic* crystal of CzDPS.

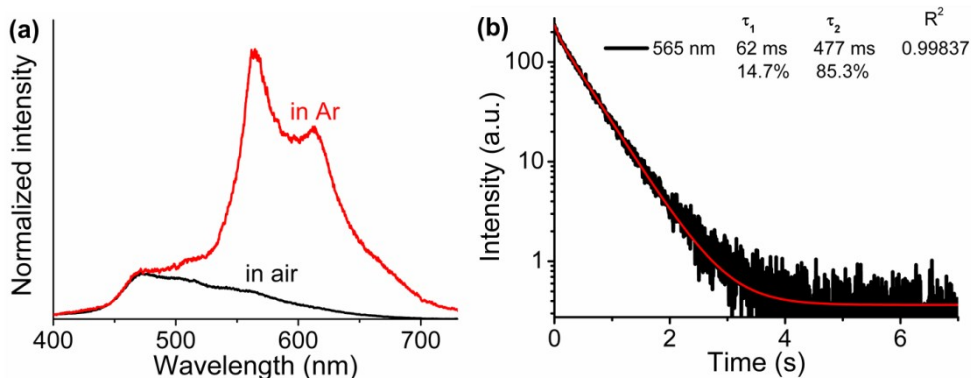


Figure S15. (a) Phosphorescence spectra of the *monoclinic* crystal of CdPS in air or Ar at room temperature, (b) Luminescence decay of the *monoclinic* crystal of CdPS in Ar. Oxygen-free environment made the luminescence spectra and decay of the *monoclinic* crystal similar to that of *orthorhombic* one.

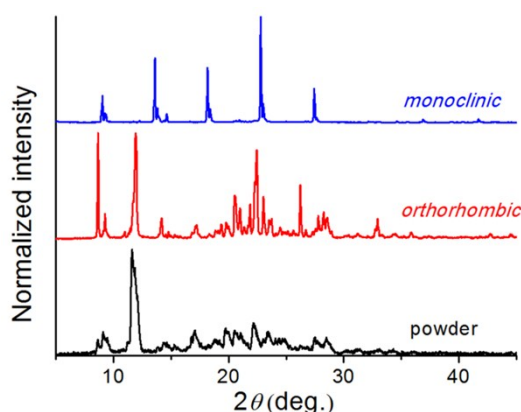


Figure S16. XRD of the *monoclinic*, *orthorhombic* and powder crystals of CdPS. The *orthorhombic* and powder crystals exhibited similar XRD spectrum, suggesting similar aggregation in the two states.

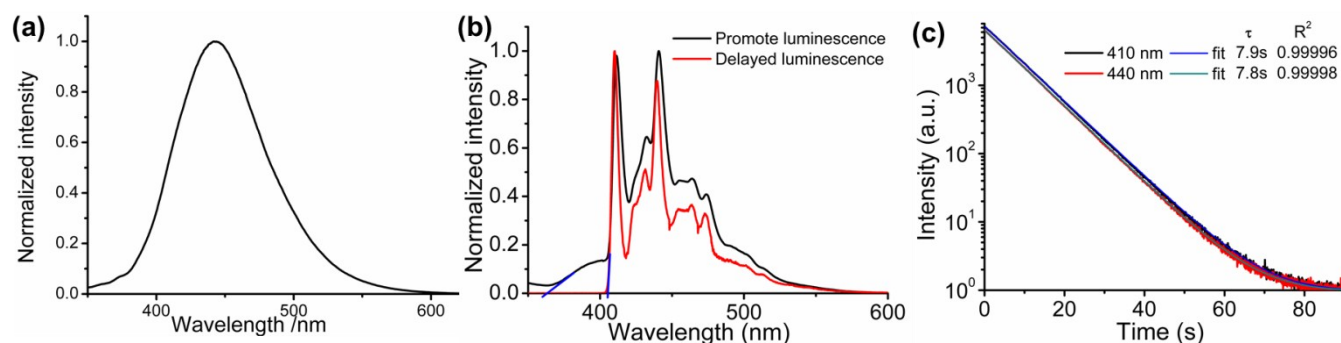


Figure S17. (a) The luminescence of 25 μM CdPS in 2-methyltetrahydrofuran at room temperature ($\lambda_{\text{ex}} = 335 \text{ nm}$). The luminescence (b) and its decay (c) of 25 μM CdPS in 2-methyltetrahydrofuran at 77K ($\lambda_{\text{ex}} = 335 \text{ nm}$). CdPS exhibited ultra-long luminescence in its dilute solution at 77K. The integral area of the delayed luminescence reached 66% of that of the promoted luminescence.

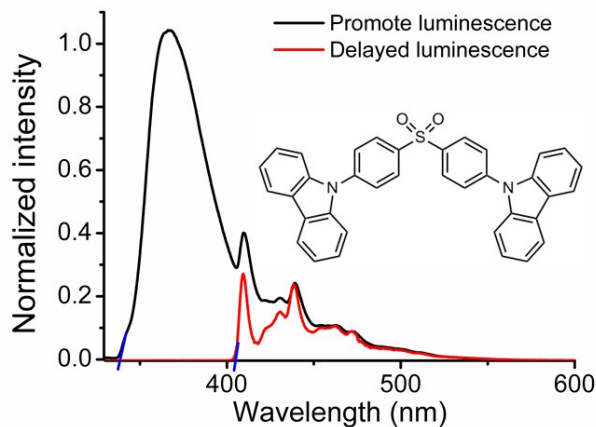


Figure S18. The luminescence of 25 μM p-CzDPS in 2-methyltetrahydrofuran at 77K ($\lambda_{\text{ex}} = 320 \text{ nm}$). p-CzDPS exhibited ultra-long luminescence in its dilute solution at 77K. According to the rising edges of the spectra, the energy level of the triplet state was estimated to be $\sim 3.06 \text{ eV}$, which was the same as that of CzDPS. But the integral area of the delayed luminescence reached only 18 % of that in the promoted luminescence, suggesting a much lower ISC efficiency than CzDPS.

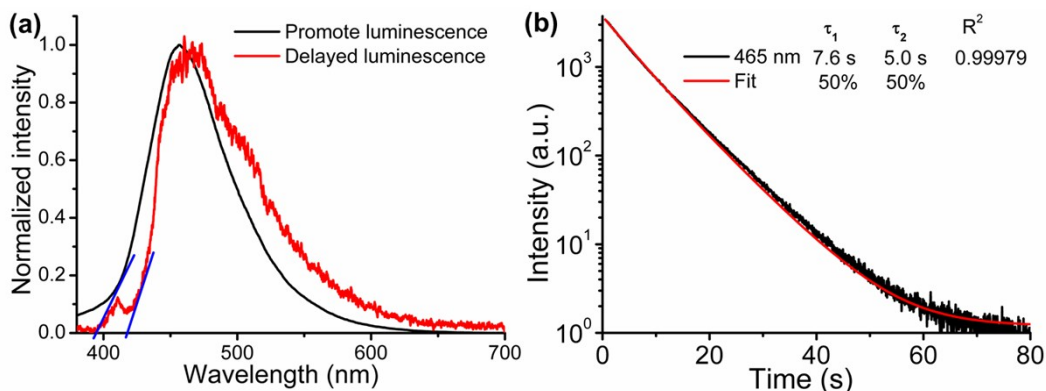


Figure S19. The luminescence spectra (a) and decay (b) of the solidified TRPGDA with 1 wt% CzDPS at 77K. The luminescence lifetime was approximate to the lifetime of CzDPS in a dilute solution at 77K.



Figure S20. Steady-state (a) and time-gated (b) luminescence images of fingerprints adhering with TPES on a piece of paper. The time-gated images were captured upon turning off the UV-LED with an exposure time of 2 s.

Table S1. Crystallographic data and structure refinements for crystal 1 and 2.

Crystal	1	2
Empirical formula	C ₃₆ H ₂₄ N ₂ O ₂ S	C ₃₆ H ₂₄ N ₂ O ₂ S
Formula weight	548.63	548.63
Temperature (K)	273(2)	296(2)
Crystal system	<i>Orthorhombic</i>	<i>Monoclinic</i>
Space group	P2(1)2(1)2(1)	P2(1)/n
a / Å	10.9667(5)	15.1171(3)
b / Å	12.3030(5)	10.6355(3)
c / Å	20.3131(12)	39.0096(9)
α(deg.)	90	90
β(deg.)	90	94.405(2)
γ(deg.)	90	90
V / Å ³	2740.7(2)	6253.4(3)
Z	4	8
F (000)	1144	2288
D _c / g·cm ⁻³	1.330	1.166
μ / mm ⁻¹	0.155	1.174
Theta range for data collection / deg.	1.9 to 28.3	2.3 to 63.1
Reflections collected / unique	26098 / 6817 [R(int) = 0.028]	8668 / 8668 [R(int) = 0.107]
Nref, Npar	6817, 371	8668, 741
Goodness-of-fit on F ²	1.011	1.273
Final R indices [I>2σ (I)]	R1 = 0.0391, wR2 = 0.1020	R1 = 0.1248, wR2 = 0.3354
(Δρ) _{max} , (Δρ) _{min} (e/Å ³)	0.16, -0.18	-0.62, 0.73

$$R_1 = \frac{[\sum(|F_o| - |F_c|)]}{\sum|F_o|}; wR_2 = \frac{[\sum[w(|F_o|^2 - |F_c|^2)^2]}{\sum[w(|F_o|^2)^2]}^{1/2}, w = 1 / [\sigma^2|F_o|^2 + (xp)^2 + yp]; \text{ where } p = \frac{[|F_o|^2 + 2|F_c|^2]}{3}.$$

Table S2. The energy levels of CzDPS from the crystal in the *Orthorhombic*, *Monoclinic* systems and the optimized geometry by TD-DFT calculations.

States	The energy level		
	<i>Orthorhombic</i>	<i>Monoclinic</i>	Optimized
S ₁	376.77 nm, 3.2907 eV	388.84 nm, 3.1885 eV	376.39 nm, 3.2940 eV
S ₂	355.10 nm, 3.4915 eV	379.32 nm, 3.2686 eV	354.99 nm, 3.4926 eV
S ₃	340.85 nm, 3.6375 eV	372.00 nm, 3.3329 eV	340.90 nm, 3.6370 eV
S ₄	332.56 nm, 3.7282 eV	371.20 nm, 3.3401 eV	332.34 nm, 3.7306 eV
S ₅	320.14 nm, 3.8728 eV	370.69 nm, 3.3447 eV	319.98 nm, 3.8748 eV
T ₁	390.02 nm, 3.1789 eV	393.25 nm, 3.1789 eV	390.16 nm, 3.1778 eV
T ₂	384.34 nm, 3.2259 eV	391.55 nm, 3.1528 eV	384.12 nm, 3.2277 eV
T ₃	378.52 nm, 3.2755 eV	384.71 nm, 3.1665 eV	378.19 nm, 3.2784 eV
T ₄	363.83 nm, 3.4077 eV	382.46 nm, 3.2228 eV	363.72 nm, 3.4088 eV
T ₅	360.28 nm, 3.4413 eV	380.62 nm, 3.2574 eV	360.16 nm, 3.4424 eV

References:

- S1** S. Xu, T. Liu, Y. Mu, Y. F. Wang, Z. Chi, C. C. Lo, S. Liu, Y. Zhang, A. Lien and J. Xu, *Angew. Chem., Int. Ed.*, 2015, 54, 874.
- S2** Z. Xie, C. Chen, S. Xu, J. Li, Y. Zhang, S. Liu, J. Xu and Z. Chi, *Angew. Chem., Int. Ed.*, 2015, 54, 7181.
- S3** K. Wu, Z. Wang, L. Zhan, C. Zhong, S. Gong, G. Xie, C. Yang, *J. Phys. Chem. Lett.* 2018, **9**, 1547.
- S4** M. J. Frisch, G. W. Trucks, H. B. Schlegel, G. E. Scuseria, M. A. Robb, J. R. Cheeseman, G. Scalmani, V. Barone, B. Mennucci, G. A. Petersson, H. Nakatsuji, M. Caricato, X. Li, H. P. Hratchian, A. F. Izmaylov, J. Bloino, G. Zheng, J. L. Sonnenberg, M. Hada, M. Ehara, K. Toyota, R. Fukuda, J. Hasegawa, M. Ishida, T. Nakajima, Y. Honda, O. Kitao, H. Nakai, T. Vreven, J. A. Montgomery, Jr., J. E. Peralta, F. Ogliaro, M. Bearpark, J. J. Heyd, E. Brothers, K. N. Kudin, V. N. Staroverov, T. Keith, R. Kobayashi, J. Normand, K. Raghavachari, A. Rendell, J. C. Burant, S. S. Iyengar, J. Tomasi, M. Cossi, N. Rega, J. M. Millam, M. Klene, J. E. Knox, J. B. Cross, V. Bakken, C. Adamo, J. Jaramillo, R.

Gomperts, R. E. Stratmann, O. Yazyev, A. J. Austin, R. Cammi, C. Pomelli, J. W. Ochterski, R. L. Martin, K. Morokuma, V. G. Zakrzewski, G. A. Voth, P. Salvador, J. J. Dannenberg, S. Dapprich, A. D. Daniels, O. Farkas, J. B. Foresman, J. V. Ortiz, J. Cioslowski, and D. J. Fox, Gaussian, Inc., Wallingford CT, 2013.

S5 L. Xu, G. Li, T. Xu, W. Zhang, S. Zhang, S. Yin, Z. An and G. He, *Chem. Commun.*, 2018, **54**, 9226.

S6 H. Ma, Q. Peng, Z. An, W. Huang and Z. Shuai, *J. Am. Chem. Soc.*, 2019, **141**, 1010.